surfaces

MDPI

Article

Technological Peculiarities of Epsilon Ferrite Epitaxial Stabilization by PLD

Polina A. Dvortsova and Sergey M. Suturin *

Division of Solid State Physics, Ioffe Institute, 26 Polytechnicheskaya, 194021 St. Petersburg, Russia
* Correspondence: suturin@mail.ioffe.ru

Abstract: The present paper describes the technological peculiarities relevant to the nucleation and further epitaxial growth of the metastable epsilon phase of iron oxide by means of pulsed laser deposition (PLD). The orthorhombic epsilon ferrite ε-Fe_2O_3 is an exotic member of a large family of iron oxide polymorphs, which attracts extensive attention nowadays due to its ultra-high magneto-crystalline anisotropy and room temperature multiferroic properties. Continuing the series of previous publications dedicated to the fabrication of ε-Fe_2O_3 films on GaN, this present work addresses a number of important requirements for the growing conditions of these films. Among the most sensitive technological parameters, the growth temperature must be high enough to aid the nucleation of the orthorhombic phase and, at the same time, low enough to prevent the thermal degradation of an overheated ε-Fe_2O_3/GaN interface. Overcoming the contradicting growth temperature requirements, an alternative substrate-independent technique to stabilize the orthorhombic phase by mild aluminum substitution is proposed. The advantages of this technique are demonstrated by the example of ε-Fe_2O_3 films PLD growth carried out on sapphire—the substrate that possesses a trigonal lattice structure and would normally drive the nucleation of the isostructural and energetically more favorable trigonal α-Fe_2O_3 phase. The real-time profiling of high-energy electron diffraction patterns has been extensively utilized throughout this work to keep track of the orthorhombic-to-trigonal balance being the most important feed-back parameter at the growth optimization stage.

Keywords: epsilon ferrite; epitaxial layers; pulsed laser deposition; electron diffraction; phase transformation

check for updates

Citation: Dvortsova, P.A.; Suturin, S.M. Technological Peculiarities of Epsilon Ferrite Epitaxial Stabilization by PLD. *Surfaces* **2022**, *5*, 445–455. https://doi.org/10.3390/surfaces5040032

Academic Editor: Gaetano Granozzi

Received: 15 September 2022
Accepted: 20 October 2022
Published: 21 October 2022

Publisher's Note: MDPI stays neutral with regard to jurisdictional claims in published maps and institutional affiliations.

Copyright: © 2022 by the authors. Licensee MDPI, Basel, Switzerland. This article is an open access article distributed under the terms and conditions of the Creative Commons Attribution (CC BY) license (https://creativecommons.org/licenses/by/4.0/).

1. Introduction

While the possibilities of traditional semiconductor electronic devices are approaching their limit, the integration of semiconductor and magnetic materials into a single heterostructure provides a promising opportunity for the development of novel functional spintronic devices. Within a large family of magnetic materials, iron oxides attract a lot of attention nowadays as they exhibit a wide variety of outstanding and not yet fully explained physical properties. Besides the fundamental interest, potential applications of iron-containing magnetically ordered materials, such as functional layers for spintronic devices (e.g., for spin filters and spin injectors), are widely discussed [1]. The multiferroic properties of complex iron oxides are well known [2–4]. Among numerous iron oxide polymorphs, the most intriguing one is the metastable orthorhombic ε-Fe_2O_3 phase, which does not exist in the bulk form. Epsilon ferrite is a ferrimagnet with a huge magneto-crystalline anisotropy that is responsible for the values of coercive force exceeding 2 T. Having attracted a lot of attention during the past few years [5–7], epsilon ferrite in the form of nanofilms [8–10] and nanoparticles [11–14] was shown to exhibit a complicated magnetic structure with four magnetic sub-lattices and room-temperature (RT) multiferroic behavior [15], which has not been observed in other simple metal oxides. Its large magnetic coercivity and proven magneto-electric coupling make this material ideal for the creation of novel oxide-based ferroic-on-semiconductor devices for spintronic applications,

including low-power consumption magnetic media storage devices [16]. Furthermore, the epitaxial growth of a room-temperature multiferroic layer with a controllable magnetization/polarization on a semiconductor provides promising opportunities to control the optical, electronic, and magnetic properties of such heterostructure by external electric and magnetic fields [17–20]. The majority of earlier papers related to ε-Fe_2O_3 were dedicated to nanoparticles [16,21,22]. The fabrication of ε-Fe_2O_3 epitaxial layers on $SrTiO_3$ (STO), Al_2O_3, and yttria-stabilized zirconia (YSZ) substrates were later demonstrated [8,15,23,24]. More recently, the possibility of the epitaxial growth of ε-Fe_2O_3 thin films on a semiconductor substrate by means of pulsed laser deposition (PLD) has been reported [9]. The magnetic properties of ε-Fe_2O_3/GaN films have been later described in detail in Refs. [10,25]. The peculiar columnar crystal structure of ε-Fe_2O_3 films has been investigated by high-resolution transmission electron microscopy (HRTEM) in planar [25] and transversal [26] geometries. Being metastable, ε-Fe_2O_3 is very sensitive to growth conditions such as the composition and pressure of the background gas, substrate temperature, and growth rate. It was demonstrated [9] that the nucleation and growth of high-quality epsilon ferrite on gallium nitride is only possible in an oxygen atmosphere at a pressure of 0.1–0.2 mbar. Decreasing oxygen pressure below 0.1 mbar leads to nucleation of a more stable trigonal α-phase of iron oxide, while increasing the pressure above 0.2 mbar results in a considerable surface roughening. The fabrication of ε-Fe_2O_3 is additionally complicated by the need to maintain a high substrate temperature of 800–830 °C as, at a lower temperature, the nucleation of a trigonal antiferromagnetic α-Fe_2O_3 phase takes place [9,25].

As discussed in the present work, a high-growth temperature, although beneficial at the nucleation stage, can result in a considerable deterioration of the nitride–oxide interface and even in the exfoliation of the grown film. Addressing the number of conflicting requirements to the growth conditions of epsilon ferrite, the present paper reveals various technological methods relevant for the stabilization of this phase on various substrates. Namely, the problem of the too-narrow temperature window is addressed by introducing a two-stage growth technique. In addition to this, taking advantage of the ability of the group III metals to substitute iron in Fe_2O_3 shifting the energy balance towards the nucleation of the orthorhombic phase, a versatile substrate-independent stabilization technique has been developed based on mild doping of the growing film with aluminum, both at the nucleation stage and during the growth. The implementation of this method is demonstrated through the technologically complex example of ε-Fe_2O_3 growth on Al_2O_3(0001)—the substrate, which is isostructural to the energetically favorable α-phase of the iron oxide.

The present paper is dedicated to the technological peculiarities of ε-Fe_2O_3 phase stabilization. Whether stabilization is effective or not is mainly judged from the real time in situ RHEED measurements. The extensive investigation of the crystal structure, surface morphology, electronic, and magnetic properties of the epsilon ferrite films grown by PLD is described elsewhere [9,10,25,26].

2. Materials and Methods

The iron oxide epitaxial films were grown on GaN/Al_2O_3 (0001) and Al_2O_3 (0001) substrates by means of a pulsed laser deposition from the stoichiometric Fe_2O_3 target, which was ablated with the pulsed radiation of a KrF excimer laser (λ = 248 nm, Coherent, COMPex Pro). The growth was performed in the PLD setup produced by SURFACE (Stuttgart, Germany). The substrate was clamped to a stainless-steel sample holder that was radiatively heated from the back with a platinum filament. The temperature of the sample holder was measured with a type-K thermocouple. The growth of epsilon ferrite was performed in an oxygen atmosphere at a pressure of 0.2 mbar, and the substrate temperature varied within the range of 600–830 °C. To carry out an aluminum substitution, the iron oxide and aluminum targets were ablated alternately. The growth rate was calibrated by means of an Inficon quartz thickness monitor to about 0.05–0.25 Å/s. The crystal structure and epitaxial relations of the grown films were monitored in situ during the growth by reflection

high energy electron diffraction (RHEED). The RHEED system was equipped with an RDEC (Ibaraki, Japan) 30 kV electron gun and homemade RHEED Capture acquisition software.

3. Results and Discussion

3.1. Tracking Orthorhombic-to-Trigonal Balance with Time Dependent RHEED Profiling

Following from the previous studies, which were dedicated to the fabrication of epitaxial ε-Fe_2O_3 layers, the stabilization of the metastable orthorhombic epsilon ferrite requires a very careful choice of growth parameters. A noticeable technological difficulty here is the irreversible nucleation of the trigonal hematite phase when the growth conditions deviate even slightly from the optimal ones. Being the most energetically stable, the α-Fe_2O_3 phase cannot simply be converted to any other crystallographic modification by tuning the basic growth parameters of oxygen pressure, growth temperature, or deposition rate. Thus, the early detection of α-Fe_2O_3 nucleation becomes the most challenging task during the epitaxial stabilization of the orthorhombic phase. When grown on GaN (0001)/Al_2O_3 (0001) or Al_2O_3 (0001), ε-Fe_2O_3 and α-Fe_2O_3 crystallize with the c-axes perpendicular to the surface. Due to similarities in the anion sublattices (Figure 1a,b), the layers of ε-Fe_2O_3 (001) and α-Fe_2O_3 (0001) can seamlessly stack on top of each other, keeping the following in-plane epitaxial relations: ε-Fe_2O_3 [100] | | α-Fe_2O_3 [110] [9]. As it will later be shown, the transition from one to the other can occur in a matter of a few nanometers. Remarkably, the reciprocal lattices of ε-Fe_2O_3 and α-Fe_2O_3 can be immediately distinguished by RHEED when viewed in an ε-Fe_2O_3 [100] = α-Fe_2O_3 [110] azimuth. The diffraction pattern of the orthorhombic ε-Fe_2O_3 phase (Figure 1d) has a twice-denser net of reflections in both in-plane and out-of-plane directions, compared to the trigonal α-Fe_2O_3 phase (Figure 1c). Thus, a convenient way to monitor mutual transformations between these phases is to record in-plane intensity profiles as indicated by the frames shown in Figure 1c,d.

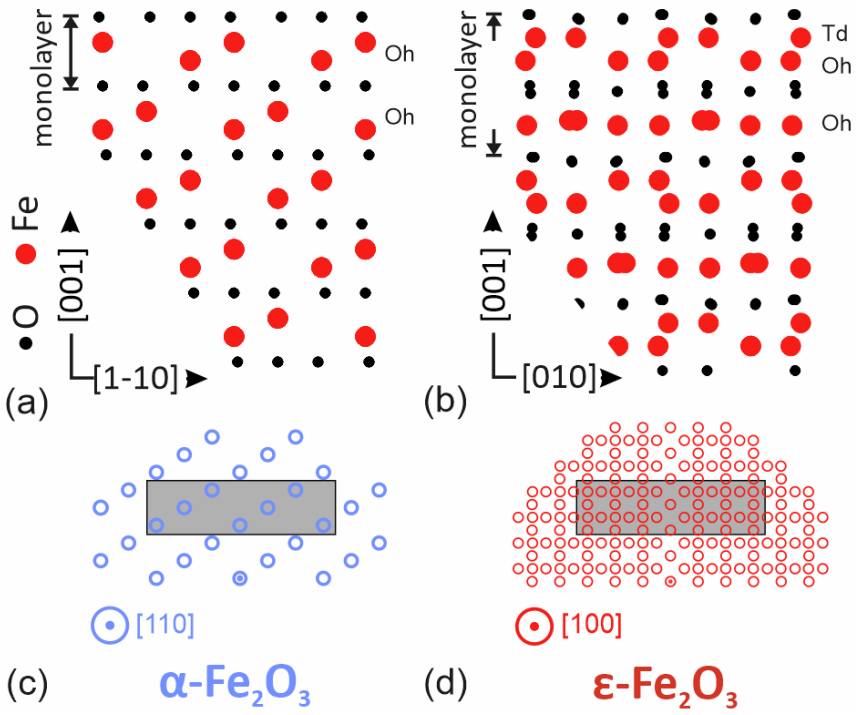

Figure 1. Crystal lattices of trigonal α-Fe_2O_3 (**a**) and orthorhombic ε-Fe_2O_3 (**b**). Reciprocal lattice cross-section of α-Fe_2O_3 (**c**) and ε-Fe_2O_3 (**d**). The reciprocal lattice nodes correspond to appearance of reflections in RHEED patterns.

The variation in the geometrical position and the intensity of the diffraction features correspond to the evolution of the crystal structure at the surface, which was monitored by plotting a time dependence of horizontal intensity profiles in the form of 2D maps, in which

the horizontal axis corresponded to the in-plane reciprocal space vector and the vertical axis corresponded to time. In this way, the very subtle changes in diffraction patterns could be effectively detected and visualized. The proposed technique is an expansion of the well-known method of recording oscillations of the specular diffraction intensity measured in a small reciprocal space region.

3.2. Gallium-Assisted Two-Stage Epitaxial Stabilization of ε-Fe_2O_3 Phase on GaN/Al_2O_3

As it was proved by a series of experiments conducted at various substrate temperatures, the crystallization of the orthorhombic ε-Fe_2O_3 phase on GaN/Al_2O_3 occurs effectively only when the substrate is kept at 800–830 °C during the nucleation stage. As it was explained in the earlier works [10,26], the nucleation of the orthorhombic phase at an elevated temperature is likely to be aided by the thermally activated diffusion of gallium [27–29] from the substrate. The intermixing of the oxidized gallium with the iron oxide results in the formation of an orthorhombic gallium iron oxide transition layer which acts as a template for the growth of isostructural ε-Fe_2O_3. Remarkably, despite the crucial role of the high substrate temperature at the nucleation stage, the growth of thicker films at 800–830 °C was found to be unfeasible due to a considerable deterioration in the crystal quality observed as the film thickness approached 100 nm. The signs of deterioration become evident from a noticeable blurring of electron diffraction patterns, which is accompanied by the appearance of whitish matte areas on the surface of the otherwise uniformly ochre film. Though the diffraction pattern gradually returns to normal once the growth is continued, the whitish areas remain constantly visible on the film surface. Moreover, in the samples thicker than 100 nm, film exfoliation occurred in the deteriorated areas once the sample was exposed to air. The observed exfoliation was most likely related to the intensified decomposition of the gallium nitride at the ε-Fe_2O_3/GaN interface triggered by the excessive heating of the substrate. The overheating naturally occurred due to the decreasing transparency of the iron oxide film as it grew thicker and more effectively absorbed the infrared radiation coming from the sample heater.

An example of a much milder interface deterioration due to Ga segregation was discussed in Refs. [10,26] dedicated to energy-dispersive X-ray spectroscopy (EDX) and polarized neutron reflectometry (PNR) studies of the sub-100 nm ε-Fe_2O_3 film grown on GaN at various temperatures. A 5 nm transition layer with a low average density and a defect-rich lattice structure was reported to form at the oxide–nitride interface of these films. Remarkably, the density depression at the interface increased noticeably with the growth temperature (down to 55% for the samples grown at 830 °C). This low density, that cannot be the property of a homogenous layer, was attributed to the presence of macroscopic voids, which (through growth and coalescence) could cause film exfoliation. The presence of such voids at the interface agrees well with the deterioration of the electron diffraction patterns due to surface corrugation, as well as with the change in the film color due to interference effects. To ensure the proper nucleation of the orthorhombic phase at the initial growth stage and, at the same time, to minimize the heat-driven interface deterioration during further deposition, a two-stage growth technology has been developed and tested. At the nucleation stage the deposition of Fe_2O_3 was carried out at a low rate of 0.05 Å/s (with an ablation frequency of 1 Hz), and the GaN substrate was kept at 830 °C.

The nucleation process was tracked by recording a time-dependent diffraction profile map (Figure 2a) that showed the evolution of diffraction intensity recorded parallel to the substrate surface within the frame shown schematically in Figure 1c,d. The growth started with the almost immediate expansion of the interstreak distance as the GaN substrate (Figure 2b) became overgrown. This expansion reflected the decrease in the in-plane periodicity from 3.19 Å in GaN to ~2.9 Å in the iron oxides. The nucleation then went through a short transition stage at which an additional 1/2 streak appeared between the main streaks. The emergence of these half-order streaks was in agreement with the presence of a defect spinel lattice in the transition layer, as observed earlier by cross-sectional HRTEM studies [26]. As the half streaks became brighter, the 1/6, 2/6, 4/6, and 5/6 streaks emerged

in the diffraction pattern and corresponded to the nucleation of the orthorhombic ε-Fe_2O_3 phase (see the modeled diffraction pattern in Figure 2c). Remarkably, a low deposition rate at this stage resulted in the faster appearance of these streaks, which was in agreement with the assumption of a surface reaction between gallium, oxygen, and iron, which took place at the beginning of the orthorhombic growth.

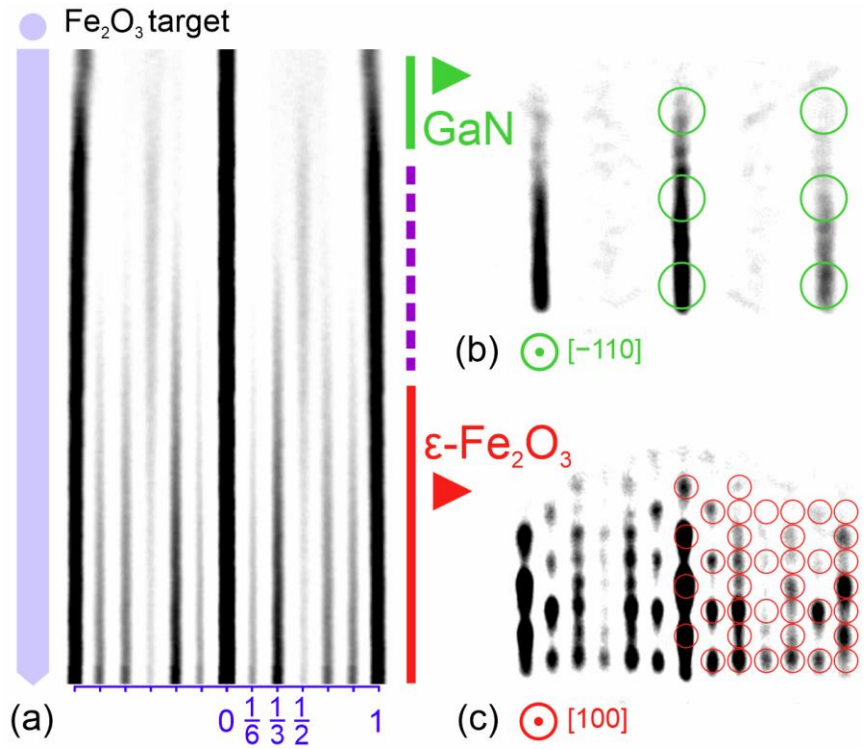

Figure 2. Time-dependent RHEED profile map (**a**) showing nucleation of the orthorhombic ε-Fe_2O_3 phase on hexagonal GaN. The map height corresponds to deposition of about 20 Å of Fe_2O_3. The corresponding RHEED patterns of GaN (**b**) and ε-Fe_2O_3 (**c**) illustrate the initial and final stages of the nucleation process.

Once the nucleation of the orthorhombic lattice became evident from the diffraction pattern, the growth rate was increased by raising the ablation frequency to 5 Hz, and the temperature of the sample holder was ramped down to prevent the excessive heating of GaN. The cooling rate was tuned to approximately 1 deg/nm to preclude overheating while still keeping the film surface temperature sufficiently high to keep the crystallization of the orthorhombic phase (as monitored by RHEED). The proposed gradual cooling was shown to be very effective for fabricating films with a thickness of up to 170 nm, including the 120 nm thick film prepared for the neutron diffraction studies presented in Ref. [25]. The resulting films had a uniform ochre color with no signs of exfoliation, and showed well-defined diffraction patterns with the reflection spots appearing in full correspondence with the reciprocal space structure of the orthorhombic ε-Fe_2O_3 (Figure 2c).

3.3. Aluminum-Assisted Stabilization of ε-Fe_2O_3 Phase on Al_2O_3

Though a high temperature at the nucleation stage is believed to be favorable for the crystallization of epsilon ferrite, heating alone does not guarantee orthorhombic growth. For example, when Fe_2O_3 is deposited on Al_2O_3 using the technological parameters derived from the well-studied ε-Fe_2O_3/GaN system (i.e., a substrate temperature of 830 °C and oxygen pressure of 0.2 mbar), the film grows with the alpha-phase iron oxide lattice as can be seen from the diffraction image shown in Figure 3b. The appearance of the trigonal hematite phase is not surprising, taking into account that α-Fe_2O_3 is not only the most stable crystallographic phase of the iron oxide but also the one isostructural to

the aluminum oxide substrate. Unlike gallium nitride, which aids ε-Fe_2O_3 nucleation by sourcing gallium, sapphire is considerably more stable and provides no source of Al into the growing film at 800–900 °C. At the same time, the presence of excessive Al is expected to help the launch of orthorhombic stabilization since all iron oxides with iron partly substituted by a group III metal (Ga, Al, In), are known to have an orthorhombic lattice. This makes it possible to stabilize the orthorhombic iron oxide phase by performing an aluminum substitution from an Al target which is ablated alternately with the iron oxide target. As the growth is performed in a 0.2 mbar of oxygen, it is assumed that the aluminum arriving from the plasma plume is oxidized to Al_2O_3 and then mixed with Fe_2O_3, forming a $Fe_{2-x}Al_xO_3$ compound on the substrate surface. The stabilization process was tracked by time-dependent RHEED profiling (Figure 3a). The process started by depositing a Fe_2O_3 5 Å/Al_2O_3 1.3 Å/Fe_2O_3 5 Å/Al_2O_3 1.3 Å/Fe_2O_3 5 Å sequence on the clean Al_2O_3 substrate. Periodic intensity oscillations were observed during the deposition while the diffraction pattern remained trigonal. Remarkably, a transition to the orthorhombic pattern was clearly observed once the aluminum/iron ratio was increased to 3:5. The nucleation occurred in a manner very similar to the one observed earlier for the Fe_2O_3/GaN system (Figure 2a). The nucleation of the 1/2 streak was followed by the appearance of 1/6, 2/6, 4/6, and 5/6 streaks. As it can be seen from the time chart shown in Figure 3a, the most dramatic trigonal-to-orthorhombic transformation occurred at the very beginning of the iron oxide deposition. The 1/3 and 2/3 streaks which are characteristic for the trigonal phase abruptly disappeared simultaneously with the appearance of the 1/2 streak. Once the n/6 streak appeared in the diffraction pattern, the growth was continued by the deposition of pure Fe_2O_3, resulting in a gradual transition to a fully developed ε-Fe_2O_3 diffraction pattern, as shown in Figure 3c.

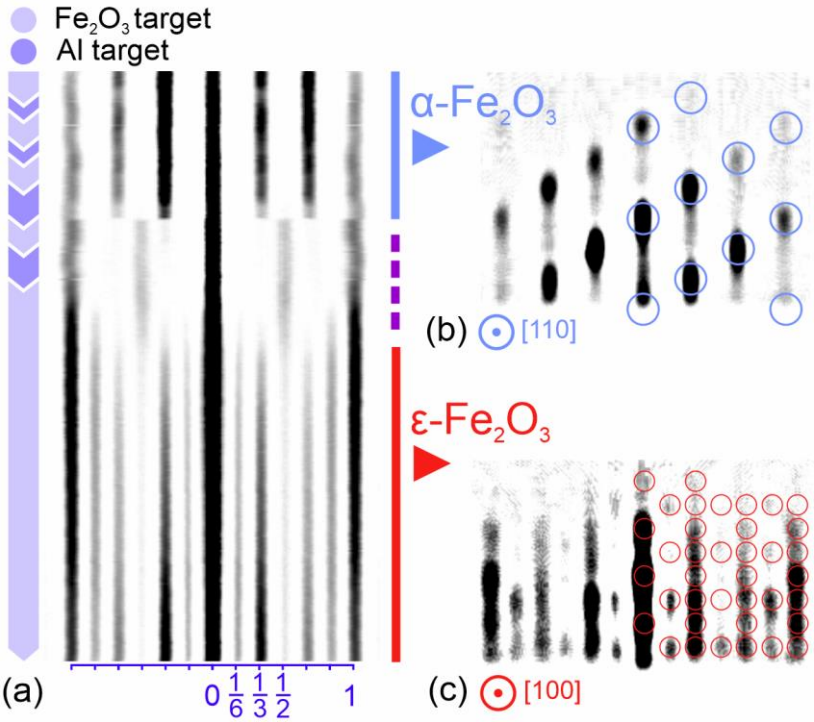

Figure 3. Time-dependent RHEED profile map (**a**) showing trigonal-to-orthorhombic transformation at the initial stage of aluminum-assisted nucleation of ε-Fe_2O_3 on Al_2O_3. The map height corresponds to deposition of about 20 Å of Fe_2O_3. The corresponding RHEED patterns of α-Fe_2O_3 (**b**) and ε-Fe_2O_3 (**c**) illustrate the initial and final stages of the nucleation process.

The estimated iron-to-aluminum ratio was maintained during the described orthorhombic stabilization corresponding to the $Al_{0.75}Fe_{1.25}O_3$ stoichiometry that is close to that of the well-known $AlFeO_3$ (AFO) compound. AFO, along with $GaFeO_3$ (GFO), has been

studied in earlier works in the form of stand-alone film and buffer layers, e.g., in Ref. [23] A 5–25 nm GFO buffer layer was used to grow the ε-Fe_2O_3 films on Al_2O_3, STO, and YSZ. The PLD growth of aluminum-substituted iron oxide onto STO and YSZ has been discussed in Ref. [30]. The $Fe_{2-x}Al_xO_3$ films were shown to preserve in-plane magnetic anisotropy but had a lower coercive field in comparison to the pure epsilon ferrite. The ferromagnetic resonance in Al and Ga-substituted orthorhombic iron oxides was studied in [31,32]. From the point of view of device applications, an important disadvantage of AFO and GFO is that their Neel temperature is below RT. On the opposite, the Neel temperature of ε-Fe_2O_3 (495 K) is far above RT, which makes it a perspective component for spintronic devices. Although mixing ε-Fe_2O_3 with Ga_2O_3 or Al_2O_3 is known to reduce the Neel temperature [33,34], using a relatively low aluminum content is supposed to keep it above RT. In what follows, the possibility of stabilizing orthorhombic growth with subtle Al substitution is demonstrated.

Interestingly, a periodic ablation of aluminum in small amounts (Al:Fe = 1:10–20) was shown to be very helpful in maintaining the orthorhombic crystal structure in thicker films which, without occasional aluminum doping, tends to switch back to trigonal. This switching is supposed to happen at defect sites, e.g., at small inclusions of the trigonal phase that are naturally present in the orthorhombic film at the column boundaries [25]. Without the suppression mechanism offered by aluminum, the small hematite inclusions grow in size until the alpha phase becomes the dominant one.

Such orthorhombic-to-trigonal transitions take place during a prolonged growth from a Fe_2O_3 target, and is shown in the top part of the profile chart presented in Figure 4a. Without Al assistance, the 1/6, 3/6, and 5/6 streaks gradually disappear, and the 1/3 and 2/3 streaks become much brighter, while the diffraction patterns corresponding to pure α-Fe_2O_3 become dominant (Figure 4b). The inverse trigonal-to-orthorhombic conversion can be carried out with a comparatively low Al:Fe ratio of 1:10, as shown in the middle part of Figure 4a. The full conversion back to orthorhombic growth was completed in five cycles with a total thickness in the transition region of about 30–40 Å. The diffraction pattern corresponded to a mixture of ε-Fe_2O_3 and α-Fe_2O_3 during the conversion (Figure 4c) and became fully orthorhombic afterwards (Figure 4d). From our experience the suggested stabilization method is the only and most effective way to suppress the nucleation of α-Fe_2O_3. Remarkably, the described trigonal-to-orthorhombic conversion can be repeated as many times as required.

3.4. The Stabilization of Orthorhombic k-Al_2O_3 Phase

Most interestingly, while a prolonged deposition of pure iron oxide onto the ε-Fe_2O_3 surface leads to the nucleation of trigonal α-Fe_2O_3, a prolonged ablation of the aluminum target onto the same surface does not produce a trigonal Al_2O_3. Unexpectedly, the diffraction pattern is gradually transformed to that of the aluminum oxide kappa phase [35,36]. This is an orthorhombic phase of Al_2O_3 with the same Pna_{21} space group and the same lattice structure as ε-Fe_2O_3.

This transformation is shown in the top part of the time-dependent profile map in Figure 5a. The transformed pattern (Figure 5c) looks very similar to that of the epsilon ferrite (Figure 5b) but is scaled by a factor of 1.05 corresponding to the smaller lattice constants of k-Al_2O_3 (a = 4.8437 Å, b = 8.3300 Å, c = 8.9547 Å). When iron oxide is deposited on top of k-Al_2O_3, the diffraction pattern returns back to that of the epsilon iron oxide. Interestingly the ε-Fe_2O_3-to-k-Al_2O_3 transition is much smoother than the reverse transition back to ε-Fe_2O_3.

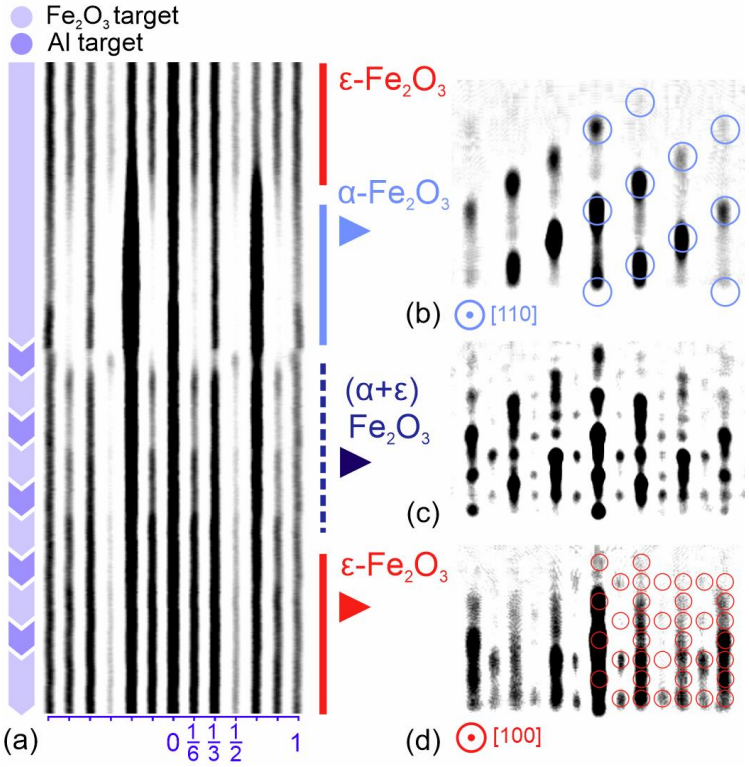

Figure 4. Time-dependent RHEED profile map (**a**) showing orthorhombic–trigonal–orthorhombic transformation. The map height corresponds to deposition of about 100 Å of Fe_2O_3. The epsilon-to-alpha transformation occurs in absence of aluminum while the reverse alpha-to-epsilon transformation takes place via 1:10 aluminum substitution carried out by consecutive ablation of Fe_2O_3 and Al targets. The RHEED pattern gradually changes during the reverse transformation from trigonal (**b**), to mixed trigonal-orthorhombic (**c**), and finally to pure orthorhombic (**d**).

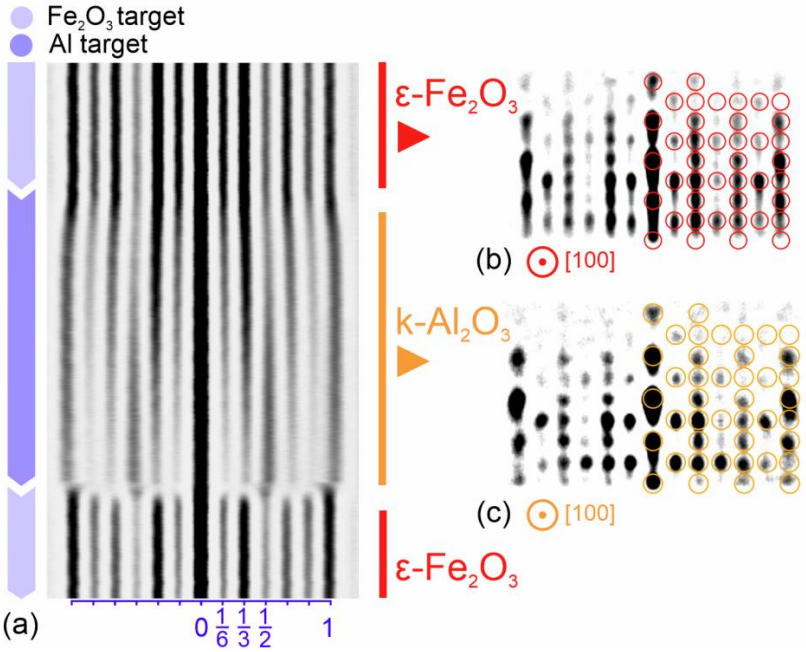

Figure 5. Time-dependent RHEED profile map (**a**) showing transformation from orthorhombic ε-Fe_2O_3 (**b**) to orthorhombic k-Al_2O_3 (**c**) taking place when Al target is ablated in 0.2 mbar of oxygen for a prolonged time. The map height corresponds to deposition of about 100 Å of Fe_2O_3. A reverse transformation takes place when k-Al_2O_3 is overgrown with Fe_2O_3.

4. Conclusions

The present paper describes the technological peculiarities relevant to the nucleation and further growth of the metastable epsilon phase of iron oxide. The main technological difficulty solved in this work is the irreversible nucleation of the trigonal hematite phase, which takes place when the growth conditions deviate from the optimal. Real-time RHEED intensity profiling was effectively implemented in this work to precisely monitor the transformations between the epsilon and alpha phases. During the initial stage of ε-Fe_2O_3 nucleation on the GaN substrate, traces of the spinel phase were observed, which appeared in the thin transition layer located at the nitride–oxide interface. To overcome the contradictory requirements for the growth temperature (which must be high enough to launch orthorhombic nucleation and low enough to prevent interface degradation), a two-stage growth technique has been introduced. An alternative substrate-independent orthorhombic phase stabilization technique based on mild aluminum substitution has also been proposed. The advantages of this method are demonstrated by the example of ε-Fe_2O_3 film growth on sapphire. It was demonstrated that the growth of the energetically favorable trigonal phase could be successfully suppressed by periodic ablation of aluminum and iron oxide targets (so that the Al content in the resulting film was below 10%). The aluminum concentration was kept low to prevent the degradation of the magnetic properties of the iron oxide. Interestingly, a prolonged ablation of the Al target onto the ε-Fe_2O_3 surface in 0.2 mbar of oxygen led to the nucleation of a rare k-Al_2O_3 phase. The discussed aluminum-assisted stabilization technique can be potentially useful for the fabrication of epsilon ferrite films on substrates with a crystal structure unfavorable for the native nucleation of the orthorhombic phase. Moreover, the same technique can be applied to growth on nitride substrates in order to launch orthorhombic nucleation at milder temperature conditions. The development of such a stable technology is believed to be important, as it can be potentially applied during the fabrication of iron-oxide-based ferroic-on-semiconductor devices with room-temperature magneto-electric coupling.

Author Contributions: Supervision and conceptualization: S.M.S.; writing: S.M.S. and P.A.D.; methodology: S.M.S. and P.A.D.; data reduction and visualization: S.M.S. and P.A.D.; review and editing: S.M.S. and P.A.D. All authors have read and agreed to the published version of the manuscript.

Funding: The authors acknowledge support from the Ministry of Science and Higher Education of the Russian Federation (agreement No. 075-15-2021-1349).

Data Availability Statement: The data presented in this study are available free of charge from the corresponding author.

Acknowledgments: The authors wish to acknowledge V. V. Lundin for providing GaN/Al_2O_3 wafers.

Conflicts of Interest: The authors declare no conflict of interest.

References

1. Li, P.; Xia, C.; Zhu, Z.; Wen, Y.; Zhang, Q.; Alshareef, H.N.; Zhang, X.-X. Ultrathin Epitaxial Ferromagnetic γ-Fe_2O_3 Layer as High Efficiency Spin Filtering Materials for Spintronics Device Based on Semiconductors. *Adv. Funct. Mater.* **2016**, *26*, 5679–5689. [CrossRef]
2. Golosova, N.O.; Kozlenko, D.P.; Kichanov, S.E.; Lukin, E.V.; Dubrovinsky, L.S.; Mammadov, A.I.; Mehdiyeva, R.Z.; Jabarov, S.H.; Liermann, H.-P.; Glazyrin, K.V.; et al. Structural, Magnetic and Vibrational Properties of Multiferroic $GaFeO_3$ at High Pressure. *J. Alloy. Compd.* **2016**, *684*, 352–358. [CrossRef]
3. Sharma, K.; Raghavendra Reddy, V.; Gupta, A.; Choudhary, R.J.; Phase, D.M.; Ganesan, V. Study of Site-Disorder in Epitaxial Magneto-Electric $GaFeO_3$ Thin Films. *Appl. Phys. Lett.* **2013**, *102*, 212401. [CrossRef]
4. Jung, J.H. Optical Magnetoelectric Absorption and Diffraction in $GaFeO_3$. *Media* **2005**, *46*, 508–512.
5. Yoshikiyo, M.; Futakawa, Y.; Shimoharai, R.; Ikeda, Y.; MacDougall, J.; Namai, A.; Ohkoshi, S. Aluminum-Titanium-Cobalt Substituted Epsilon Iron Oxide Nanosize Hard Magnetic Ferrite for Magnetic Recording and Millimeter Wave Absorption. *Chem. Phys. Lett.* **2022**, *803*, 139821. [CrossRef]
6. Cleron, J.; Baker, A.A.; Nakotte, T.; Troksa, A.; Han, J. Exploring Critical Synthetic Parameters for Nanoscale ε-Fe_2O_3 and Their Influence on Magnetic Behaviors. *J. Phys. Chem. C* **2022**, *126*, 7256–7263. [CrossRef]

7. López-Sánchez, J.; Serrano, A.; del Campo, A.; Muñoz-Noval, Á.; Salas-Colera, E.; Cabero, M.; Varela, M.; Abuín, M.; Castro, G.R.; Rubio-Zuazo, J.; et al. A Combined Micro-Raman, X-Ray Absorption and Magnetic Study to Follow the Glycerol-Assisted Growth of Epsilon-Iron Oxide Sol-Gel Coatings. *J. Alloy. Compd.* **2021**, *892*, 162061. [CrossRef]
8. Gich, M.; Gazquez, J.; Roig, A.; Crespi, A.; Fontcuberta, J.; Idrobo, J.C.; Pennycook, S.J.; Varela, M.; Skumryev, V.; Varela, M. Epitaxial Stabilization of ε-Fe_2O_3 (00l) Thin Films on $SrTiO_3$ (111). *Appl. Phys. Lett.* **2010**, *96*, 112508. [CrossRef]
9. Suturin, S.M.; Korovin, A.M.; Gastev, S.V.; Volkov, M.P.; Sitnikova, A.A.; Kirilenko, D.A.; Tabuchi, M.; Sokolov, N.S. Tunable Polymorphism of Epitaxial Iron Oxides in the Four-in-One Ferroic-on-GaN System with Magnetically Ordered α-, γ-, ε-Fe_2O_3 and Fe_3O_4 Layers. *Phys. Rev. Mater.* **2018**, *2*, 073403. [CrossRef]
10. Ukleev, V.; Suturin, S.; Nakajima, T.; Arima, T.; Saerbeck, T.; Hanashima, T.; Sitnikova, A.; Kirilenko, D.; Yakovlev, N.; Sokolov, N. Unveiling Structural, Chemical and Magnetic Interfacial Peculiarities in ε-Fe_2O_3/GaN (0001) Epitaxial Films. *Sci. Rep.* **2018**, *8*, 8741. [CrossRef]
11. Gich, M.; Roig, A.; Frontera, C.; Molins, E.; Sort, J.; Popovici, M.; Chouteau, G.; Martín y Marero, D.; Nogués, J. Large Coercivity and Low-Temperature Magnetic Reorientation in ε-Fe_2O_3 Nanoparticles. *J. Appl. Phys.* **2005**, *98*, 044307. [CrossRef]
12. Tokoro, H.; Fukui, J.; Watanabe, K.; Yoshikiyo, M.; Namai, A.; Ohkoshi, S. Crystal Growth Control of Rod-Shaped ε-Fe_2O_3 Nanocrystals. *RSC Adv.* **2020**, *10*, 39611–39616. [CrossRef]
13. Gu, Y.; Yoshikiyo, M.; Namai, A.; Bonvin, D.; Martinez, A.; Piñol, R.; Téllez, P.; Silva, N.J.O.; Ahrentorp, F.; Johansson, C.; et al. Magnetic Hyperthermia with ε-Fe_2O_3 Nanoparticles. *RSC Adv.* **2020**, *10*, 28786–28797. [CrossRef]
14. Klekotka, U.; Satuła, D.; Kalska-Szostko, B. ε-Phase of Iron Oxide out of Thermally Treated Magnetite Nanoparticles. *J. Magn. Magn. Mater.* **2020**, *497*, 165999. [CrossRef]
15. Gich, M.; Fina, I.; Morelli, A.; Sánchez, F.; Alexe, M.; Gàzquez, J.; Fontcuberta, J.; Roig, A. Multiferroic Iron Oxide Thin Films at Room Temperature. *Adv. Mater.* **2014**, *26*, 4645–4652. [CrossRef]
16. Ohkoshi, S.-I.; Namai, A.; Imoto, K.; Yoshikiyo, M.; Tarora, W.; Nakagawa, K.; Komine, M.; Miyamoto, Y.; Nasu, T.; Oka, S.; et al. Nanometer-Size Hard Magnetic Ferrite Exhibiting High Optical-Transparency and Nonlinear Optical-Magnetoelectric Effect. *Sci. Rep.* **2015**, *5*, 14414. [CrossRef]
17. Scott, J.F. Multiferroic Memories. *Nat Mater* **2007**, *6*, 256–257. [CrossRef]
18. Gajek, M.; Bibes, M.; Fusil, S.; Bouzehouane, K.; Fontcuberta, J.; Barthélémy, A.; Fert, A. Tunnel Junctions with Multiferroic Barriers. *Nat. Mater.* **2007**, *6*, 296–302. [CrossRef]
19. Ortega, N.; Kumar, A.; Scott, J.F.; Katiyar, R.S. Multifunctional Magnetoelectric Materials for Device Applications. *J. Phys. Condens. Matter* **2015**, *27*, 504002. [CrossRef]
20. Hu, J.-M.; Duan, C.-G.; Nan, C.-W.; Chen, L.-Q. Understanding and Designing Magnetoelectric Heterostructures Guided by Computation: Progresses, Remaining Questions, and Perspectives. *NPJ Comput. Mater.* **2017**, *3*, 18. [CrossRef]
21. López-Sánchez, J.; Serrano, A.; Del Campo, A.; Abuín, M.; Rodríguez de la Fuente, O.; Carmona, N. Sol–Gel Synthesis and Micro-Raman Characterization of ε-Fe_2O_3 Micro- and Nanoparticles. *Chem. Mater.* **2016**, *28*, 511–518. [CrossRef]
22. Namai, A.; Yoshikiyo, M.; Yamada, K.; Sakurai, S.; Goto, T.; Yoshida, T.; Miyazaki, T.; Nakajima, M.; Suemoto, T.; Tokoro, H.; et al. Hard Magnetic Ferrite with a Gigantic Coercivity and High Frequency Millimetre Wave Rotation. *Nat. Commun.* **2012**, *3*, 1035. [CrossRef] [PubMed]
23. Thai, T.M.N.; Nguyen, D.T.; Lee, N.-S.; Rhyee, J.-S.; Song, J.; Kim, H.-J. Stabilization of Metastable ε-Fe_2O_3 Thin Films Using a $GaFeO_3$ Buffer. *J. Appl. Phys.* **2016**, *120*, 185304. [CrossRef]
24. Corbellini, L.; Lacroix, C.; Harnagea, C.; Korinek, A.; Botton, G.A.; Ménard, D.; Pignolet, A. Epitaxially Stabilized Thin Films of ε-Fe_2O_3 (001) Grown on YSZ (100). *Sci. Rep.* **2017**, *7*, 3712. [CrossRef] [PubMed]
25. Suturin, S.M.; Korovin, A.M.; Sitnikova, A.A.; Kirilenko, D.A.; Volkov, M.P.; Dvortsova, P.A.; Ukleev, V.A.; Tabuchi, M.; Sokolov, N.S. Correlation between Crystal Structure and Magnetism in PLD Grown Epitaxial Films of ε-Fe 2 O 3 on GaN. *Sci. Technol. Adv. Mater.* **2021**, *22*, 85–99. [CrossRef]
26. Suturin, S.M.; Dvortsova, P.A.; Snigirev, L.A.; Ukleev, V.A.; Hanashima, T.; Rosado, M.; Ballesteros, B. Structural Peculiarities of ε-Fe_2O_3/GaN Epitaxial Layers Unveiled by High-Resolution Transmission Electron Microscopy and Neutron Reflectometry. *Mater. Today Commun.* **2022**, *33*, 104412. [CrossRef]
27. Sun, C.J.; Kung, P.; Saxler, A.; Ohsato, H.; Bigan, E.; Razeghi, M.; Gaskill, D.K. Thermal Stability of GaN Thin Films Grown on (0001) Al_2O_3, (01$\bar{1}$2) Al_2O_3 and $(0001)_{Si}$ 6H-SiC Substrates. *J. Appl. Phys.* **1994**, *76*, 236–241. [CrossRef]
28. Huang, S.; Gu, S.; Tang, K.; Ye, J.; Xu, Z.; Zhu, S.; Zheng, Y. Influence of Oxygen Precursors and Annealing on Fe_3O_4 Films Grown on GaN Templates by Metal Organic Chemical Vapor Deposition. *J. Vac. Sci. Technol. B Nanotechnol. Microelectron. Mater. Process. Meas. Phenom.* **2014**, *32*, 052801. [CrossRef]
29. Xu, Z.; Huang, S.; Tang, K.; Gu, S.; Zhu, S.; Ye, J.; Xu, M.; Wang, W.; Zheng, Y. The Compositional, Structural, and Magnetic Properties of a Fe_3O_4/Ga_2O_3/GaN Spin Injecting Hetero-Structure Grown by Metal-Organic Chemical Vapor Deposition. *Appl. Surf. Sci.* **2016**, *388*, 141–147. [CrossRef]
30. Corbellini, L.; Lacroix, C.; Ménard, D.; Pignolet, A. The Effect of Al Substitution on the Structural and Magnetic Properties of Epitaxial Thin Films of Epsilon Ferrite. *Scr. Mater.* **2017**, *140*, 63–66. [CrossRef]
31. Ohkoshi, S.; Kuroki, S.; Sakurai, S.; Matsumoto, K.; Sato, K.; Sasaki, S. A Millimeter-Wave Absorber Based on Gallium-Substituted ε-Iron Oxide Nanomagnets. *Angew. Chem. Int. Ed.* **2007**, *46*, 8392–8395. [CrossRef]

32. Namai, A.; Sakurai, S.; Nakajima, M.; Suemoto, T.; Matsumoto, K.; Goto, M.; Sasaki, S.; Ohkoshi, S. Synthesis of an Electromagnetic Wave Absorber for High-Speed Wireless Communication. *J. Am. Chem. Soc.* **2009**, *131*, 1170–1173. [CrossRef]
33. Ohkoshi, S.; Namai, A.; Sakurai, S. The Origin of Ferromagnetism in ε-Fe_2O_3 and ε-$Ga_xFe_{2-x}O_3$ Nanomagnets. *J. Phys. Chem. C* **2009**, *113*, 11235–11238. [CrossRef]
34. Saha, R.; Shireen, A.; Shirodkar, S.N.; Waghmare, U.V.; Sundaresan, A.; Rao, C.N.R. Multiferroic and Magnetoelectric Nature of GaFeO3, AlFeO3 and Related Oxides. *Solid State Commun.* **2012**, *152*, 1964–1968. [CrossRef]
35. Ollivier, B.; Retoux, R.; Lacorre, P.; Massiot, D.; Férey, G. Crystal Structure of κ-Alumina: An X-Ray Powder Diffraction, TEM and NMR Study. *J. Mater. Chem.* **1997**, *7*, 1049–1056. [CrossRef]
36. Smrčok, L.; Langer, V.; Halvarsson, M.; Ruppi, S. A New Rietveld Refinement of κ-Al_2O_3. *Z. Krist. Cryst. Mater.* **2001**, *216*, 409–412. [CrossRef]